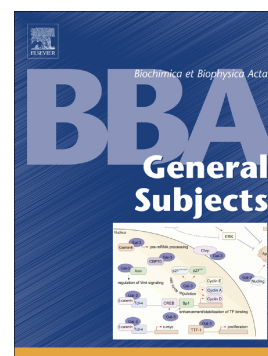


Mutations of key substrate binding residues of leishmanial peptidase T alter its functional and structural dynamics

Saleem Yousuf Bhat, Insaf Ahmed Qureshi



PII: S0304-4165(19)30251-X

DOI: <https://doi.org/10.1016/j.bbagen.2019.129465>

Reference: BBAGEN 129465

To appear in: *BBA - General Subjects*

Received date: 3 August 2019

Revised date: 15 October 2019

Accepted date: 24 October 2019

Please cite this article as: S.Y. Bhat and I.A. Qureshi, Mutations of key substrate binding residues of leishmanial peptidase T alter its functional and structural dynamics, *BBA - General Subjects*(2019), <https://doi.org/10.1016/j.bbagen.2019.129465>

This is a PDF file of an article that has undergone enhancements after acceptance, such as the addition of a cover page and metadata, and formatting for readability, but it is not yet the definitive version of record. This version will undergo additional copyediting, typesetting and review before it is published in its final form, but we are providing this version to give early visibility of the article. Please note that, during the production process, errors may be discovered which could affect the content, and all legal disclaimers that apply to the journal pertain.

Mutations of key substrate binding residues of leishmanial peptidase T alter its functional and structural dynamics

Saleem Yousuf Bhat and Insaf Ahmed Qureshi*

Department of Biotechnology & Bioinformatics, School of Life Sciences, University of Hyderabad, Prof. C.R. Rao Road, Hyderabad 500046, India

*Correspondence e-mail: insaf@uohyd.ac.in

Journal Pre-proof

Abstract

Background: M20 aminopeptidases, such as Peptidase T (PepT), are implicated in the hydrolysis of oligopeptides during the terminal stages of protein degradation pathway to maintain turnover. Therefore, specific inhibition of PepT bores well for the development of novel next-generation antileishmanials. This work describes the metal dependence, substrate preferences and inhibition of PepT, and demonstrates in detail the role of its two conserved substrate binding residues.

Methods: PepT was purified and characterized using a scheme of peptide substrates and peptidomimetic inhibitors. Residues T364 and N378 were mutated and characterized with an array of biochemical, biophysical and structural biology methods.

Results: PepT sequence carries conserved motifs typical of M20 peptidases and our work on its biochemistry shows that this cytosolic enzyme carries broad substrate specificity with best cleavage preference for peptides carrying alanine at the P¹ position. Peptidomimetics amastatin and actinonin occupied S¹ pocket by competing with the substrate for binding to active site and inhibited PepT potently while arphamenine A and bestatin were less effective inhibitors. We further show that the mutation of conserved substrate binding residues (T364 and N378) to alanine affects structure, reduces substrate binding and alters the amidolytic activity of this dimeric enzyme.

Conclusions: PepT preferentially hydrolyzes oligopeptides carrying alanine at P¹ position and is potently inhibited by peptidomimetics. Reduced substrate binding after mutations was a key factor involved in amidolytic digressions.

General significance: This study provides insights for further exploration of the druggability of PepT and highlights prospective applications of this enzyme along with its mutazyme T364A/N378A.

Keywords: Peptidase T; Substrate binding site; Mutazymes; Biotechnological applications

1. Introduction

Cytosolic proteolysis is a vital cellular process for its role in amino acid metabolism, progression of cell cycle [1], quality control [2] and the adjustment of the turnover of regulatory molecules [3]. Besides, it is crucial for physiological processes like gene expression [4] and antigen presentation [5] in living systems. In eukaryotes, the major pathway responsible for the turnover of intracellular proteins is the ubiquitin-proteasome complex [6]. After ubiquitination, the proteins to be degraded are unfolded before their entry

into the large multi-subunit complex termed as the 26S proteasome in the cytosol and nucleus. The 26S proteasome is composed of two 19S regulatory complexes and a cylindrical 20S proteasomal core which is proteolytically active. The ubiquitinated substrates enter 26S proteasome through narrow pores in the 20S proteasomal core and are degraded through a process that requires ATP hydrolysis [7, 8].

The degradation of proteins is believed to occur via endoproteolytic cleavages yielding shorter peptides [9, 10], which are further broken by multiple cytosolic exopeptidases into tripeptides and dipeptides [11, 12]. In fact, the cytosolic exopeptidases are regarded as essential components of the protein degradation system as these enzymes act as scavengers of the oligopeptides generated by the ATP-dependent endoproteases during protein degradation [13]. However, the cytosolic aminopeptidases (exopeptidases) act in an ATP-independent manner on their substrates [14]. Based on evolutionary relationships, the peptidases are grouped into 86 families viz. serine, threonine, cysteine, aspartate, glutamate and metallo-peptidases [15]. Amongst metallo-peptidases, M20 family enzymes are responsible for the hydrolysis of amino acid residues from N-terminal end of proteins and synthetic peptides [16]. These enzymes are involved in diverse functions in living systems ranging from the hydrolysis of late products of protein degradation to protein maturation, tissue repair, and cell-cycle control [16, 17]. The viability of these enzymes renders them highly relevant for biotechnological or therapeutical applications. For example, aminopeptidase V (PepV) from *Lactobacillus* sp. and *Salmonella typhimurium* peptidase T (PepT) function in amino acid utilization [18, 19]. Other members of M20 peptidases like *Escherichia coli* allantoate amido-hydrolase [20] and yeast alanine synthase (AS) [21] are necessary for the nucleotide catabolic pathway. Furthermore, *E. coli* K12 peptidase D (PepD) exhibit dipeptidase activity on unusual dipeptides such as L-carnosine (Ala-His) and L-homocarnosine (amino-butyl-His), as well as on a few other distinct tripeptides highlighting the importance of M20 aminopeptidases in free amino acid regulation [16]. While the M20 succinyl-diaminopimelate desuccinylase from the human gut pathogen *H. pylori* is considered a potential candidate for therapeutic intervention [22], another M20 aminopeptidase of *Pseudomonas* sp. strain RS-16 carboxypeptidase G2 (CPG2) is currently being used to develop antibody-directed enzyme pro-drug therapy [23].

The MEROPS peptidase database classifies M20 family of metallo-peptidases as "co-catalytic" type as two metal ions bind per monomer of protein with broad substrate specificity. Five residues of protein bind to or interact with two metals in the active site with one of the residues ligating with both metal ions. The active site general arrangement of M20

peptidases is: His/Asp, Asp, Glu, Glu/Asp, His [19]. However, variations are expected in the general active site in individual subfamilies. The previous reports on enzyme catalysis of M20 enzymes highlights striking role of two catalytic zinc ions in the stabilization of the tetrahedral intermediate and activation of the catalytic water molecule [16, 19]. The protein data bank (PDB) houses many M20 family crystal structures viz. structure of Peptidase T from *S. typhimurium* [19] and *E. coli* (PDB ID: 1FNO), PepV from *Lactobacillus delbrueckii* [24], CPG2 from *Pseudomonas* sp. strain RS-16 [25] and CN2 from mice [26]. All M20 family metallo-enzyme structures reported till date have a two domain organization and exist mainly as homodimers [25] with the exception of PepV which is a monomer [24]. Although many M20 family metallo-enzyme structures are now available in the PDB, general biochemistry including metal dependence and substrate preferences of these enzymes remain unstudied. There is also no report that describes whether these enzymes can be modified with the use of protein engineering or molecular biology to develop peptidases with better industrial or therapeutic value.

We herein present a detailed structural and biochemical characterization of M20 PepT from *Leishmania donovani* and reflect on the roles of conserved PepT family substrate binding residues with site directed mutagenesis. We show that PepT is active when the conserved T364 and N378 residues are mutated to Ala and that one mutant enzyme transforms into an efficient broad-spectrum aminopeptidase. With surface plasmon resonance, biochemical and molecular dynamics studies, we highlight the mechanism of amidolytic disparity and altered kinetic parameters. Furthermore, this report highlights that the modification of important or conserved substrate binding residues of PepT may yield an enzyme with a broad range of substrate preferences which may increase its potential industrial and medicinal applications.

2. Methodology

2.1 Sequence analysis and homology modelling

The *Leishmania donovani* Peptidase T (PepT) sequence was retrieved from online database KEGG (<https://www.genome.jp/kegg/>) and subjected to sequence and domain analysis using multiple web-based bioinformatics programs. Localization of PepT sequence was predicted using the program Euk-mPLoc 2.0 [27].

To generate molecular models of PepT and mutazymes T364A, N378A and T364A/N378A with program Modeller [28], crystal structure of Peptidase T from *E. coli* (PDB ID: 1VIX) was selected as the structural template (sequence identity with the template, 41%). The loops in the modelled structures were refined with Modloop [29] and all models were energy minimized with the program Gromacs [30]. Structural coordinates of all structures were

validated with the program RAMPAGE [31] and the molecular visualization carried out in PyMol [32].

2.2 Molecular cloning and site directed mutagenesis

PepT ORF of 1298 nucleotides was amplified from the genomic DNA of *L. donovani* with gene specific primers (forward primer 5' ATAGCTAGCATGTCTCTCGCGCCGATCGAACAC 3' and reverse primer 5' ACTAAGCTTCTACAGCAAGGACGGCGTCCTCTTG 3'). The amplicon was purified, digested with enzymes *NheI* and *HindIII* and cloned into the expression vector pET28a. Simultaneously, conserved substrate binding residues (T364 and N378) of PepT sequence were mutated to alanine using primers containing a mutation. The mutations were carried out by inverse PCR method using a PCR program as follows: 98 °C for 30 seconds, 98 °C for 30 seconds, 55/60 °C for 1 minute, 68 °C for 7 minutes and 72 °C for 10 minutes. The reaction was subjected to *DpnI* digestion for 1 h at 37 °C to digest the methylated template DNA to ensure all transformants observed harbour a mutated plasmid. All mutations were confirmed by DNA sequencing.

2.3 Protein expression and purification

For the expression of PepT and mutazymes, *E. coli* BL21 (DE3) cells were used. Bacterial cultures were grown in LB medium containing 50 mg/l of kanamycin at 37 °C until A₆₀₀ reached to 0.5. IPTG was added to a final concentration of 0.4 mM and the culture grown for next 20 hours at 18 °C in a shaking incubator. Cells were harvested by centrifugation at 8000 rpm for 20 minutes and resuspended in lysis buffer 50 mM Tris–HCl (pH 8.0), 400 mM KCl, 25 mM imidazole, 10% (v/v) glycerol, 1 mM PMSF and 1 mM DTT. Lysozyme was added in a ratio of 1:50 and the resuspension incubated on ice for 1 hour. Finally, cells were disintegrated by sonication and the cell lysate centrifuged at 14000 rpm for 40 minutes at 4 °C. The supernatant was then loaded into a 50 ml jacketed column for protein binding into a pre-packed Ni-NTA column (GE Life Sciences). After initial washes with low concentration of imidazole to remove non-specificities, the protein was finally eluted with a buffer bearing 300 mM imidazole. The protein quality was checked on a 10% (w/v) SDS-PAGE. As an extra-purification step and to study oligomerization, best protein fractions were directly loaded onto a pre-calibrated Sephadex G-200 HR gel-filtration column (GE Life Sciences) equilibrated with running buffer composed of 50 mM Tris–HCl (pH 8.0), 150 mM KCl and 2 mM DTT.

2.4 CD and fluorescence spectroscopic measurements and heat denaturation assays

CD spectra of PepT and its mutazymes T364A, N378A and T364A/N378A were recorded at room temperature on JASCO-J1500 CD spectropolarimeter in a quartz cell with a path length of 0.2 cm. The spectropolarimeter was set to accumulate three scans for each spectrum at a scan speed of 50 nm min⁻¹. Data was collected at every nanometer from 250 to 200 nm with final concentration of proteins maintained at 5 µM in 10 mM potassium phosphate buffer (pH 7.2) and 25 mM NaCl. To study thermo-stability, spectral changes of PepT and mutazymes were recorded in the temperature range of 293 to 353 K. The spectral data was normalized and plotted against temperature (K) to gather a sigmoidal curve. Thermodynamic parameters were determined using two-state equilibrium unfolding model in Sigma plot 12.0 (San Jose, USA). The secondary structure content of four enzymes was computed using the K2D algorithm of the program DICHROWEB (<http://dichroweb.cryst.bbk.ac.uk/>). For spectrofluorometry with Horiba FluoroMax-3 spectrofluorometer, 1 µM of PepT and mutazymes was taken in 10 mM phosphate buffer (pH 7.2)-100 mM NaCl and the spectra was recorded at room temperature using excitation and emission slit width of 5 nm. All enzymes were excited at 280 nm and the emission recorded from 300-400 nm.

2.5 Aminopeptidase assays and inhibition studies

The aminopeptidase activity kinetics of PepT and mutazymes T364A, N378A and T364A/N378A was performed by a continuous kinetic method using fluorogenic peptide substrates linked to fluorophore 7-amido-4-methylcoumarin (AMC) solubilised in DMSO. The final concentration of DMSO in the kinetic assays was less than 2 percent. Fluorescence emission due to the hydrolysis of AMC from Ala-AMC, Leu-AMC, Met-AMC, Arg-AMC, Lys-ala-AMC, Ala-leu-Lys-AMC and Ala-ala-phe-AMC was monitored during a 60 minute kinetic cycle on TECAN Infinite M200 Pro Spectrofluorometer with a break of 5 minutes between measurements. The λ_{ex} and λ_{em} pairs used to monitor the release of AMC were as per the recommendations of manufacturer (Sigma-Aldrich). The metal profile was generated using a metal supplementation of 0 to 10 mM. Using optimum metal concentration of each metal, kinetic assays were carried out with an enzyme concentration of 0.3 µM at 37 °C in a 96 well plate in the assay buffer composed of 50 mM Tris-HCl (pH 7.2) and 20 µM of Co(II). Enzyme activity was measured in the substrate concentration range of 0-600 µM with each well blanked by its respective substrate concentration while data plotting. The pH profile for protein activity was generated as reported previously [33] with standard buffers in the pH range of 4-10 using acetate, MES, Tris-HCl and CAPS buffers. Steady state kinetic parameters were determined by converting fluorescence to product formation (AMC) using an AMC standard curve. All parameters were determined in Graphpad prism 5.0. We tested

inhibitors bestatin, arphamenine A, amastatin and actinonin and determined the mode of action, inhibition constant (K_i) and IC-50 values for every inhibitor with PepT and its mutazymes. For mode of action, Lineweaver-Burk method was used while K_i was computed by plotting the slope (K_m/V_{max}) of uninhibited and inhibited curves against inhibitor concentrations used in the kinetic assays. IC-50 values were determined by variable slope method in Graphpad Prism (San Diego, USA).

2.6 Surface Plasmon Resonance (SPR) binding assays

SPR (Biacore) assays were conducted at room temperature using a CM-5 dextran chip (GE Healthcare) coupled covalently to ligands PepT and point mutant N378A (30 μ g/ml each) via amine coupling. The matching running and injection buffers consisted of 1X PBS (pH 7.4) and 0.005% P-20. All analytes (substrates of PepT and mutazyme N378A) in 2% DMSO were injected at a final concentration of 200 μ M measuring response units (RU) as a function of concentration of analytes at a flow rate of 30 μ l/min. Kinetic analysis was carried out with Biacore T200 evaluation software 2.0 following a 1:1 Langmuir binding model after necessary solvent corrections.

2.7 Molecular docking

Molecular docking was performed with Autodock Vina [34] to unravel the molecular interactions of substrates and inhibitors with PepT and its mutazymes whose structures were modelled and validated. The structural coordinates of inhibitors and peptide substrates were drawn manually, energy minimized, and their geometry optimized as reported previously [33]. The ligand coordinates were used to generate Autodock inbuilt files with Autodock tools (ADT). Before defining the binding site, water molecules and hydrogens were removed. Polar hydrogens were added and the grid configured around the catalytic residues of PepT and its mutazymes with dimensions 36x26x34. LigPlot analysis and PyMol [32] were used to decipher atomic interactions.

2.8 Molecular dynamics

Molecular dynamics simulations were executed with Gromacs [30] using GROMOS96 43a1 as a force field and SPC as water model for 40 ns for PepT and its mutants (T364A, N378A and T364A/N378A). The MDS was also run for the complexes of these enzymes with the most favourable substrate Ala-AMC to understand the disparity in kinetic attributes of all enzymes. For complexes, the docking conformation with highest binding affinity was selected. The topology and itp files for Ala-AMC was generated from PRODRG server and added to PepT and its mutants topology files to generate complex topologies. All systems were solvated and the charges neutralized by adding sodium ions to each system. The electro-

neutral systems generated were energy minimized by steepest descent method to obtain stability and abate steric clashes. All systems were subjected to two canonical equilibration runs to stabilize the temperature and pressure factors as shown previously [33] before a production MD run of 40 ns for data collection was started.

3. Results

3.1 PepT is a member of M20 family of aminopeptidases

To investigate the similarity between *Leishmania donovani* PepT and PepT sequences from other organisms, multiple sequence alignment was carried out. Initial examination of the leishmanial PepT sequence revealed it to be a member of M20 aminopeptidases which mostly exist as functional dimers. Domain organization of this enzyme is given in Figure 1A.

The leishmanial PepT shows a significant similarity with *E. coli* and *S. typhimurium* PepT sequences and doesn't have close ortholog in *Homo sapiens*. The alignment of leishmanial PepT sequence with those of *E. coli*, *B. anthracis* and *S. typhimurium* PepT sequences reveal the functional domains especially the zinc-binding and substrate binding site to be highly conserved between these three sequences (Figure 1B). The active site residues composed of two histidines, two aspartates and a glutamate is conserved between *L. donovani* PepT and peptidase T sequences from *S. typhimurium* [19] and *E. coli* (PDB ID: 1FNO). Simultaneously, localization predictions suggested PepT enzyme to be cytosolic like its other member from *S. typhimurium* [35].

For structural insights, homology structural models of PepT and its mutazymes were generated and validated. The dimeric modelled structure (Figure 1C) encompasses two monomers, each composed of 423 residues and aligned into two functional domains: an N terminal catalytic domain which carries the zinc binding motif HXDT and a C-terminal lid domain for protein dimerization. Lid domain of each monomer utilizes hydrophobic interactions and an extensive hydrogen bonding network between two PepT monomers to give rise to a dimeric interface. Additionally, the substrate binding residues T364 and N378 of peptidase T from *S. typhimurium* and *E. coli* and other known crystallographic peptidase T structures were found conserved and located in the signature motif $X_1X_2RGGTDGXXLSXXGLXXPN$ within the substrate binding site. Amongst the five active site residues, two aspartates and a glutamate are found in direct association with two zinc ions in catalytic centre with glutamate making a contact with both metal ions (Figure 1D). While aligning the modelled structures of PepT and mutazymes it was observed that mutation of Thr364 and Asn378 to alanine induced RMSD differences and rotameric changes in the metal binding residues (Figure 1E).

3.2 Purification of PepT and its mutazymes T364A, N378A and T364A/N378A

The full length PepT from *L. donovani* was cloned into the expression vector pET28a. After confirmation of clone with DNA sequencing and generation of mutants T364A, N378A and T364A/N378A, all plasmids were transformed into *E. coli* BL21 (DE3) cells for expression. Consequently, all proteins were purified by Ni-NTA affinity chromatography and found to be a single band of approximately 49 kDa with 95% purity on SDS-PAGE (Figure 2A). The elution profiles of PepT in gel filtration chromatography and the simultaneous analysis of the partition coefficients (k_{av}) of PepT with the known partition coefficients (k_{av}) of standard proteins suggested PepT to be a homo-dimer in solution (Figure 2B).

3.3 Mutations alter PepT secondary structure

Circular dichroism spectroscopy was used to determine the secondary structure of PepT and understand the changes in average secondary structure after mutations. The multiple far-UV CD spectra recorded for both PepT and mutazymes suggested slight changes in the average secondary structure (Figure 2C). The analysis of experimental CD data with K2D algorithm suggested mutations reducing the α -helical content and leading to a concomitant increase in the percentage of β -sheets (Table 1). Heat denaturation assays indicated both mutations to have decreased the thermostability (Figure 2D). Florescence spectra of all enzymes showed emission to be maximal at 324 nm suggesting aromatic residues were buried in the hydrophobic interior and all enzymes exhibited comparable conformational states (Figure 2E).

3.4 PepT is a functional metal dependent alanine aminopeptidase

All known metal dependent aminopeptidases require divalent metal ions for activity. This is true for all metal dependent aminopeptidases characterized thus far with noted ones being the M24 methionine aminopeptidases [36] and M17 leucine aminopeptidase [37]. Using a pH and temperature gradient, we firstly obtained the optimal pH (pH 7.5) and temperature (37°C) for aminopeptidase assays (Figure 3A, B). Consequently, eight different metal chlorides were tested in the aminopeptidase assays at their optimum concentration which was determined by incubating PepT with all metal chlorides in the concentration range of 0-10 mM (Figure 3C). Amongst eight metal chlorides [Co(II), Mn(II), Mg(II), Ca(II), Ni(II), Zn(II), Cu(II) and Fe(II)], divalent cobalt emerged as the most efficient activator of PepT followed by manganese, calcium and magnesium albeit at different optimal concentrations. While as,

cobalt was a major activator in low concentrations (10-50 μM), magnesium and calcium activated PepT best in millimolar concentrations. On the contrary, PepT didn't show much activity with Zn(II) or Cu(II) in micromolar concentrations. Therefore, these metals were used in nanomolar concentrations to obtain optimal activity (Figure 3D). The optimal metal ion concentrations and kinetic parameters determined for PepT with the supplementation of different metal chlorides at physiological pH are given in Table 2. Since Co(II) emerged as the major activator of PepT and mutazymes (T364A, N378A and T364A/N378A), all aminopeptidase assays were carried out with the supplementation of 20 μM Co(II) in the assay buffer.

Initially, the aminopeptidase activity of PepT and mutazymes was tested against Ala-AMC in a kinetic cycle at 37°C for 1 hour. All enzymes exhibited highest activity towards Ala-AMC albeit with contrasting turnover (Figure 3E). Native PepT released Ala with highest turnover. This data indicated that the *L. donovani* PepT encodes a functional M20 alanine aminopeptidase in the form of PepT and that the mutation of T364 and N378 with Ala didn't inactivate the PepT. To ascertain whether PepT and mutazymes can cleave other amino acid residues, other fluorogenic substrates were tested in the aminopeptidase assays. Although the recombinant PepT and its mutazymes cleaved both Leu and Met, turnover was significantly low suggesting the PepT didn't favour the catalysis of residues with higher radius of gyration or larger side-chains (Figure 3F-G). As PepT has a negatively charged catalytic core, its catalytic efficiency for the hydrolysis of basic residue Arg was tested. Indeed, PepT cleaved Arg with higher efficiency from Arg-AMC. However, the Arg hydrolysis was low for mutazymes except T364A/N378A which cleaved Arg with a higher turnover (Figure 3H). Interestingly, the turnover of T364A/N378A against all substrates was higher than point mutants and emerged as mutazyme with broader substrate specificity. Unlike native PepT, T364A and N378A, mutazyme T364A/N378A cleaved bigger residues at P¹ position with higher catalytic efficiency from oligopeptides (Figure 3I-K). We witnessed low turnover of PepT against tripeptides not carrying Ala in the P¹ position (Figure 3J-K) suggesting PepT to be specific to peptides carrying Ala in the P¹ position (Figure 3I). Intriguingly, both point mutations rendered PepT catalytically inefficient as turnover of point mutants (T364A and N378A) against all substrates including dipeptides and tripeptides was low. The steady state kinetic parameters of PepT and mutazymes against all tested peptides are summarized in Table 3.

3.5 Peptidomimetic inhibitors actinonin and amastatin inhibit PepT potently

PepT does not have a close ortholog in *Homo sapiens* and therefore can be an exciting molecular target against leishmaniasis. This led us to test multiple aminopeptidase inhibitors in inhibition assays to find a potent inhibitor of this enzyme. We tested inhibitors arphamenine A, bestatin, amastatin and actinonin which inhibit many aminopeptidases including the most widely studied members of M17 aminopeptidases [37, 38].

The results showed that inhibitors arphamenine A, bestatin, amastatin and actinonin inhibit PepT and its mutants T364A, N378A and T364A/N378A in a dose-dependent manner (Figure 4A, E, I, M). While estimating the inhibition constant (K_i) for all inhibitors, it was found that amastatin and actinonin had K_i in low nanomolar range (Figure 4B, F, J, N) suggesting their higher affinity for PepT than aminopeptidase inhibitors arphamenine A and bestatin whose K_i values were 4.37 μ M and 76.6 μ M, respectively. Like native PepT, all mutazymes were vulnerable to inhibition by arphamenine A, bestatin, actinonin and amastatin (Figure 3C, G, K, O and Table 4). A progressive increase in K_m and a steady V_{max} suggested all tested inhibitors acting through a competitive mode of inhibition, a concept fully augmented by molecular (flexible) docking studies which suggested the binding of inhibitors occurring at the PepT active site or co-catalytic core through hydrogen bonding and hydrophobic interactions with the catalytic and S^1 and S^1' subsite residues (Figure 4D, H, L, P). The inhibitor-enzyme contacts were maximal for the complexes of PepT with amastatin and actinonin arrayed through intensive hydrogen bonding network enabling complete occupation of the PepT catalytic centre and the substrate binding pocket.

3.6 Peptide substrates bind strongly to native PepT than N378A

To assess the sharp decline in the amidolytic activity of PepT mutants, native enzyme (PepT) and mutazyme (N378A) was covalently immobilized on a CM5 sensor chip. Using substrates Lys-ala-AMC, Ala-leu-lys-AMC and Met-AMC as analytes, we monitored the level of interaction between ligands (PepT and N378A) and substrate analytes. Results showed a direct interaction between analytes and ligands with substrates Ala-leu-lys-AMC and Lys-ala-AMC binding best amongst analytes to both PepT and N378A. However, the interaction was more pronounced and stable when substrates bound to PepT than to N378A as the resonance units (RU) were greater for the interaction between substrates and PepT (Figure 5A-D). The kinetic analysis with increasing concentration of analytes showed that Lys-ala-AMC and Ala-leu-lys-AMC bound with poor affinity to N378A and displayed high off-rate unlike PepT which showed low off-rate and a stabler binding with Lys-ala-AMC (Table 5). The results suggested a perturbation of substrate binding pocket by mutations, poor substrate binding and

a possible misorientation of the substrates in mutazyme N378A enabling poor hydrolysis of peptide bonds. This possibly explains the digressions observed in the aminopeptidase assays when conserved T364 and N378 are mutated to Ala. The same may be true for other mutazymes as they showed a somewhat similar trend in aminopeptidase assays. Leu-AMC and Met-AMC were poorly hydrolyzed by PepT, therefore, using Met-AMC as an analyte of both ligands (PepT and point mutant N378A) we found a weak association and high degree of dissociation between Met-AMC and protein ligands (Figure 5E and F). The dissociation was highly pronounced for N378A supporting the conclusion that mutations reduce substrate binding and explaining the poor activity of PepT against Met-AMC.

3.7 Dimeric assembly restricts the substrate preferences of PepT to smaller residues

To understand the structural basis of substrate specificity, molecular docking was performed. Substrates Ala-AMC (Figure 6A) and Lys-ala-AMC (Figure 6B) docked with PepT at its catalytic active site with multiple hydrogen bonds and hydrophobic interactions occupying S¹ pocket with high binding energy (-7.1 and -6.8 kcal/mol). Substrates with a bulkier P¹ residue (such as Ala-ala-phe-AMC) had binding energies comparable to Ala-AMC due to hydrogen bonding and plenteous hydrophobic interactions at the substrate entry site but failed to protrude into the catalytic site and underwent misorientation (Figure 6C), which explains the poor turnover of PepT against such substrates. Thus, dimeric assembly repels larger substrates and renders PepT specific to peptides possessing smaller P¹ residue such as Ala (Figure 4K).

3.8 Structural basis of disparity in PepT amidolytic activity after mutations

Molecular dynamics simulations were used to study the stability of PepT and its mutazymes (T364A, N378A and T364A/N378A) in native forms and in complex with Ala-AMC by utilising group parameters like root mean square deviation (RMSD), root mean square fluctuation (RMSF) and the radius of gyration (Rg). The 20 ns production run was further used to compute the binding energy of all enzymes in complex with Ala-AMC using Molecular Mechanics Poisson-Boltzmann Surface Area (MM/PBSA) free energy calculations approach.

RMSD was plotted from 0 to 40 ns to assess the convergence of enzyme structures to equilibrium during the production run. The RMSD plot of PepT and its complex reached to equilibrium towards the end of MDS. However, the PepT-Ala-AMC complex showed comparatively lesser RMS deviations than the native PepT (Figure 7A) asserting lesser

structural changes after substrate binding and a stable complex formation. A similar trend in RMSD was observed for mutants T364A, N378A and T364A/N378A and their complexes with Ala-AMC (Figure 7E, M). On the contrary, RMSD of N378A was greatest amongst all enzymes between 20 to 30 ns signifying the mutation to cause a structural aberration. The enzyme also appeared to be partially unfolded and reached to equilibrium only after 30 ns during the course of MD run indicating N378 to be important for the maintenance of structural integrity. Interestingly, the complex of N378A with Ala-AMC didn't show any major deviation in RMSD after Ala-AMC binding suggesting the stabilizing effect of substrate on the structure of N378A (Figure 7I). The flexibility during the 40 ns MDS run was estimated by plotting RMSF of all enzymes and their complexes. All enzyme-substrate complexes had lower fluctuations than the native PepT, T364A, N378A and T364A/N378A (Figure 7B, F, J, N). The partial unfolding observed in N378A due to mutation appeared to have dampened, demonstrating high complex stability after substrate binding.

The compactness of all systems was assessed by Rg against time (Figure 7C, G, K, and O). Rg which describes the overall mobility of atomic assemblies stood steady for every system during MDS except a slight increase observed in T364A-Ala-AMC complex. The Rg or compactness was not identical for all systems. While as, all group parameters including Rg displayed an overall stabilizing effect of peptide substrate Ala-AMC binding to native PepT and mutazymes, Rg demonstrated a partial protein unfolding like behaviour for point mutants T364A and N378A towards the end of production run (Figure 7G, K) which could be a contributing factor to the less aminopeptidase activity observed by these point mutants. Overall, group parameters pointed towards major structural changes after mutations of key substrate binding residues implying towards the cruciality of conserved T364 and N378 not just for substrate binding but to maintain structural integrity of M20 aminopeptidases.

Furthermore, the binding free energy values of all enzyme- substrate complexes during the 40 ns production run indicated that Ala-AMC possesses a negative binding energy with all enzymes. However, the substrate Ala-AMC had the highest average binding energy with native PepT suggesting a better association or affinity of Ala-AMC with the native PepT than mutants (Figure 7Q). The results are in agreement with surface plasmon resonance binding assays which suggested the occurrence of a stable high order bimolecular interaction of substrates with native PepT and not with mutazyme N378A. Pertinently, PepT and T364A/N378A showed better cleavage efficiency for Ala in aminopeptidase assays than point mutants T364A and N378A. Therefore, the molecular dynamics studies provide structural basis for high catalytic efficiency of PepT over mutazymes and explains the

disparity in amidolytic activity of PepT after mutations. Conversely, MD simulations asserted hydrogen bonding and hydrophobic interactions (Figure 7D, H, L and P) to be responsible for holding the substrate Ala-AMC in the active sites of all enzymes which corroborates with the molecular docking results.

4. Discussion

Aminopeptidases are ubiquitous metal dependent exopeptidases that release amino acids from proteins or peptides from their N-terminus [40]. These enzymes play diverse roles in parasite biology and have recently been investigated as drug targets in parasitic infections [22, 41-42]. Aminopeptidases confer disease resistance [43], virulence [44] and can be crucial for pathogen survival [22]. The M17 leucine aminopeptidase localized to the *Leishmania* cytosol is required for free amino acid regulation via its aminopeptidase activity [37]. Therefore, it is possible that PepT has a similar role as it hydrolyzes oligopeptides in the cytoplasm and acts on the exogenously supplied peptides [19, 35] thereby, enabling the parasite to acquire free amino acid residues for its protein biosynthesis and the maintenance of turnover.

We firstly demonstrate that PepT is expressed in properly folded form and catalyzes the cleavage of amino acids from the synthetic fluorogenic peptide substrates with the supplementation of divalent metal ions. The divalent cobalt proved to be a major activator of PepT activity which can be attributed to the formation of low spin and high coordination complexes by cobalt [45, 46]. PepT showed high turnover and catalytic efficiency against peptides carrying alanine at P¹ position and had a poor turnover against peptides with a larger P¹ residue due to the hindrance caused by the dimeric interface. This suggests PepT to be specific for the release of alanine from oligopeptides in the cytosol. This mechanism is somewhat similar to the one observed in M17 leucine aminopeptidases (LAPs) where the hexameric assembly limits the substrate preferences of LAP to preferential leucine or methionine hydrolysis [39]. Bioinformatics analysis predicted this enzyme to be cytosolic. The presence of a single copy number of PepT and lack of its close ortholog in *Homo sapiens* may thus offer a lucrative opportunity to target this aminopeptidase so as to dismantle the protein turnover in leishmanial cytoplasm and limit parasite growth. This led us to develop an *in vitro* inhibition assay to find a potent inhibitor for this enzyme. Bestatin and arphamenine A exhibited less potency towards PepT than M17 leucine aminopeptidases [37] possibly because these two aminopeptidases have different active site architecture and catalytic residue topologies. However, much like M17 leucine aminopeptidases, the inhibitors amastatin and actinonin inhibited PepT potently in low nanomolar concentrations through a

competitive mode of inhibition mediated through extensive hydrogen bonding network and hydrophobic interactions [38]. Higher potency of actinonin and amastatin suggests these molecules to be useful scaffolds for the designing of novel small molecule inhibitor libraries for the selective inhibition of PepT to combat a spectrum of human diseases caused by parasites belonging to trypanosomatids.

The crystal structures of PepT from *S. typhimurium* [19], *E. coli* (PDB ID: 1FNO) and the modelled structure of *L. donovani* PepT points towards the conservation of two residues (T364 and N378) in the substrate binding site apart from the conserved metal bridging site identified through the superimposition of LAP-amastatin complex [47] and APP-phenylalanine hydroxamate complex [48]. The substrate binding site of PepT carries a highly conserved characteristic glycine rich fingerprint motif as $X_1X_2RGGTDG$ which distinguishes this family of enzymes from other MH clan peptidases [41]. The X_1 and X_2 are P and M in PepT, respectively. The replacement of conserved residues T364 and N378 with Ala led to the sharp decline in activity suggesting T364 and N378 to be important for substrate recognition and positioning. However, a double mutant where both T364 and N378 were replaced with Ala retained significant turnover number for the release of Ala. The point mutants T364A and N378A had a deleterious effect on catalytic efficiency for the release of Ala, Leu and Met unlike T364A/N378A whose overall kinetic parameters were better than both point mutants (T364A and N378A). It is possible that the presence of smaller Ala residue in places of charged residues T364 and N378 led to the expansion of the substrate binding pocket and thence accommodated larger substrate residues like Met or Leu better than point mutants T364A and N378A. It is also possible that the presence of alanine in the places of T364 and N378 led to the dramatic changes in the substrate binding environment of PepT which may have caused the subtle orientation shift of the bound substrate. This could in turn lead to the change of distance between the substrate and the catalytic residues and alter substrate preferences. To further explain changes in turnover (k_{cat}) after mutations, molecular dynamics studies were conducted for all enzyme-substrate complexes; it was observed that substrate Ala-AMC possesses a negative binding energy with all enzymes throughout the 40 ns production run. However, the negative binding energy of substrate was comparatively higher with native PepT suggesting a better binding of Ala-AMC with the native PepT than all mutazymes. This is in a greater agreement with the binding profiles observed for PepT and N378A through surface plasmon resonance. All substrates had a stable binding with PepT than to N378A suggesting the mutations to have reduced the affinity of PepT substrate binding pocket for peptide substrates. This in turn highlights the important roles of T364 and

N378 for substrate binding and explains the fall in amidolytic activity of N378A and other mutants.

Additionally, all mutazymes showed differences in the secondary structure content and were less thermo-stable in the thermal denaturation assays than the native PepT. This asserts that the mutations modulated the adjacent secondary structure which may have rendered mutazymes less thermo-stable than the native PepT. Mutazyme N378A showed least thermostability possibly due to its unstable behaviour as suggested by higher RMSD. Less thermostability of mutants can also be attributed to their slight loss of helical content [49]. The major changes in RMSD and RMSF in particular for mutazyme N378A suggests key substrate binding residues T364 and N378 to be crucial for the maintenance of structural integrity. Pertinently, the aminopeptidase activity of single mutants declined several folds for every substrate suggesting the mutation to be transmitting a deleterious effect on its catalytic site. Therefore, amidolytic digressions after mutations may be a consequence of secondary structural changes as well.

The PepT structural fold resembles that of the hexameric LAP [30], CG2 [25] and APP [40]. However, the second domain of LAP which holds the subunits together is absent in PepT sequences including leishmanial PepT as well as CG2 [25]. Instead, the dimeric PepT and CG2 carry a second domain of over 100 residues which provides dimeric inter-chain contacts to the two monomeric units of PepT and CG2. This is in agreement with the results of gel filtration chromatography results which suggest *L. donovani* PepT to be a homo-dimer in solution. Intriguingly, the Peptidase T enzymes from different living systems elute as monomers [50, 51], dimers [52] and even trimers [53]. Alternatively, molecular modelling of leishmanial PepT suggested dimerization contacts between its two monomers to be similar to that of *S. typhimurium* Peptidase T [19] and CG2 [25]. It consists of an antiparallel β -strand alignment involving residues Ala273-Ser279 (Ala264-Val270 in *S. typhimurium* Peptidase T and Ala268-Ala270 in CG2, respectively). Additionally, it comprises of an anti-parallel α -helical coiled coil together with a large segment of amino acid residues (Lys237-Cys262) surrounding this helix. Therefore, similar to CG2 [25] and *S. typhimurium* Peptidase T [19], the dimerization domains of two PepT monomers make up a continuous eight-stranded antiparallel β -sheet.

This study highlights the purification, metal promiscuity, metal dependence, enzyme characteristics, substrate preferences and structural dynamics of M20 PepT from *L. donovani*. As many of these enzymes are considered validate targets for drug design we through biochemical assays found potent inhibitors of this enzyme and provide insights into their

mechanism of inhibition. While noting that one of the major challenges in protein engineering is to generate enzymes of broad-spectrum specificity and high turnover, we engineered a PepT double mutant (T364A/N378A) which displays higher amidolytic activity and broader substrate preferences. Amidolytic assays, surface plasmon resonance and MD simulations suggested lesser substrate binding to be a key factor behind declining turnover of point mutants. Due to broader substrate specificity and promising catalytic efficiencies, PepT and its mutazyme (T364A/N378A) may find a potential use in biotechnology, industry and medicine.

5. Acknowledgements

We are thankful to Prof. Swati Saha and Dr. Irfan A. Ghazi for providing genomic DNA of *L. donovani* and extending support for this study, respectively. We also thank to Dr. Praveen of Proteomics facility, UoH for technical help during SPR binding assays. We acknowledge Indian Council of Medical Research (ICMR) for Senior Research Fellowship (SRF) to SYB. We also acknowledge the instruments facilities supported by DST-FIST and UGC-SAP to the Department of Biotechnology & Bioinformatics, and Bioinformatics Infrastructure Facility, School of Life Sciences, University of Hyderabad, Hyderabad for computational resources.

6. Declarations of interest

The authors declare that they have no competing interests.

7. Funding information

This work is supported by a grant awarded to IAQ from Council of Scientific and Industrial Research [CSIR, project no. 37(1686)/17/EMR-II], Government of India.

8. Author contributions

SYB performed all the experiments, analysed the data and drafted the manuscript. IAQ conceptualized and supervised the study, and refined the manuscript.

9. References

1. Pagano, M. (1997) Cell cycle regulation by the ubiquitin pathway. *FASEB J.* **11**, 1067-75.
2. Amm, I., Sommer, T. and Wolf, D.H. (2014) Protein quality control and elimination of

- protein waste: the role of the ubiquitin-proteasome system. *Biochim Biophys Acta*. **1843**, 182-96.
3. Schubert, U., Antón, L.C., Gibbs, J., Norbury, C.C., Yewdell, J.W. and Bennink, J.R. (2000) Rapid degradation of a large fraction of newly synthesized proteins by proteasomes. *Nature*. **404**, 770-4.
 4. Pahl, H.L. and Baeuerle, P.A. (1996) Control of gene expression by proteolysis. *Curr Opin Cell Biol*. **8**, 340-7.
 5. Rock, K.L., Gramm, C., Rothstein, L., Clark, K., Stein, R., Dick, L., et al. (1994) Inhibitors of the proteasome block the degradation of most cell proteins and the generation of peptides presented on MHC class I molecules. *Cell*. **78**, 761-71.
 6. Goldberg, A.L., Akopian, T.N., Kisselev, A.F., Lee, D.H. and Rohrwild, M. (1997) New insights into the mechanisms and importance of the proteasome in intracellular protein degradation. *Biol Chem*. **378**, 131-40.
 7. Ciechanover, A. (1994) The ubiquitin-proteasome proteolytic pathway. *Cell*. **79**, 13-21.
 8. Coux, O., Tanaka, K. and Goldberg, A.L. (1996) Structure and functions of the 20S and 26S proteasomes. *Annu Rev Biochem*. **65**, 801-47.
 9. Emmerich, N.P., Nussbaum, A.K., Stevanovic, S., Priemer, M., Toes, R.E., Rammensee, H.G. et al. (2000) The human 26 S and 20 S proteasomes generate overlapping but different sets of peptide fragments from a model protein substrate. *J Biol Chem*. **275**, 21140-8.
 10. Kisselev, A.F., Akopian, T.N., Woo, K.M. and Goldberg, A.L. (1999) The sizes of peptides generated from protein by mammalian 26 and 20 S proteasomes. Implications for understanding the degradative mechanism and antigen presentation. *J Biol Chem*. **274**, 3363-71.
 11. Botbol, V. and Scornik, O.A. (1991) Measurement of instant rates of protein degradation in the livers of intact mice by the accumulation of bestatin-induced peptides. *J Biol Chem*. **266**, 2151-7.
 12. Ferro, E.S., Hyslop, S. and Camargo, A.C. (2004) Intracellular peptides as putative natural regulators of protein interactions. *J Neurochem*. **91**, 769-77.
 13. Yao, T. and Cohen, R.E. (1999) Giant proteases: beyond the proteasome. *Curr Biol*. **9**,

R551-3.

14. Schoehn, G., Vellieux, F.M., Asunción Durá, M., Receveur-Bréchet, V., Fabry, C.M., Ruigrok, R.W., et al. (2006) An archaeal peptidase assembles into two different quaternary structures: A tetrahedron and a giant octahedron. *J Biol Chem.* **281**, 36327-37.
15. Barrett, A.J. (1994) Classification of peptidases. *Methods Enzymol.* **244**, 1-15.
16. Chang, C.Y., Hsieh, Y.C., Wang, T.Y., Chen, Y.C., Wang, Y.K., Chiang, T.W., et al. (2010) Crystal structure and mutational analysis of aminoacyl histidine dipeptidase from *Vibrio alginolyticus* reveal a new architecture of M20 metallopeptidases. *J Biol Chem.* **285**, 39500-10.
17. Chen, S.L., Marino, T., Fang, W.H., Russo, N. and Himo, F. (2008) Peptide hydrolysis by the binuclear zinc enzyme aminopeptidase from *Aeromonas proteolytica*: a density functional theory study. *J Phys Chem B.* **112**, 2494-500.
18. Hellendoorn, M.A., Franke-Fayard, B.M., Mierau, I., Venema, G. and Kok, J. (1997) Cloning and analysis of the pepV dipeptidase gene of *Lactococcus lactis* MG1363. *J Bacteriol.* **179**, 3410-5.
19. Håkansson, K. and Miller, C.G. (2002) Structure of peptidase T from *Salmonella typhimurium*. *Eur J Biochem.* **269**, 443-50.
20. Xi, H., Schneider, B.L. and Reitzer, L. (2000) Purine catabolism in *Escherichia coli* and function of xanthine dehydrogenase in purine salvage. *J Bacteriol.* **182**, 5332-41.
21. Xu, Y.F., Létisse, F., Absalan, F., Lu, W., Kuznetsova, E., Brown, G., et al. (2013) Nucleotide degradation and ribose salvage in yeast. *Mol Syst Biol.* **9**, 665.
22. Karita, M., Etterbeek, M.L., Forsyth, M.H., Tummuru, M.K. and Blaser, M.J. (1997) Characterization of *Helicobacter pylori* dapE and construction of a conditionally lethal dapE mutant. *Infect Immun.* **65**, 4158-64.
23. Melton, R.G., Searle, F., Sherwood, R.F., Bagshawe, K.D. and Boden, J.A. (1990) The potential of carboxypeptidase G2: antibody conjugates as anti-tumour agents. II. *In vivo* localising and clearance properties in a choriocarcinoma model. *Br J Cancer.* **61**, 420-4.
24. Jozic, D., Bourenkow, G., Bartunik, H., Scholze, H., Dive, V., Henrich, B., et al. (2002) Crystal structure of the dinuclear zinc aminopeptidase PepV from *Lactobacillus delbrueckii* unravels its preference for dipeptides. *Structure.* **10**, 1097-106.

25. Rowsell, S., Paupit, R.A., Tucker, A.D., Melton, R.G., Blow, D.M. and Brick, P. (1997) Crystal structure of carboxypeptidase G2, a bacterial enzyme with applications in cancer therapy. *Structure*. **5**, 337-47.
26. Unno, H., Yamashita, T., Ujita, S., Okumura, N., Otani, H., Okumura, A., et al. (2008) Structural basis for substrate recognition and hydrolysis by mouse carnosinase CN2. *J Biol Chem*. **283**, 27289-99.
27. Chou, K.C. and Shen, H.B. (2010) A new method for predicting the subcellular localization of eukaryotic proteins with both single and multiple sites: Euk-mPLoc 2.0. *PLoS One*. **5**, e9931.
28. Sali, A. (2008) MODELLER A Program for Protein Structure Modeling Release 9v4, r6262. <http://salilab.org/modeller>.
29. Fiser, A. and Sali, A. (2003) ModLoop: automated modeling of loops in protein structures. *Bioinformatics*. **19**, 2500-1.
30. Van Der Spoel, D., Lindahl, E., Hess, B., Groenhof, G., Mark, A.E. and Berendsen, H.J. (2005) GROMACS: fast, flexible, and free. *J Comput Chem*. **26**, 1701-18.
31. Wang, W., Xia, M., Chen, J., Deng, F., Yuan, R., Zhang, X., et al. (2016) Data set for phylogenetic tree and RAMPAGE Ramachandran plot analysis of SODs in *Gossypium raimondii* and *G. arboreum*. *Data Brief*. **9**, 345-8.
32. DeLano, W.L. (2002) The PyMOL Molecular Graphics System. Schrödinger LLC www.pymol.org Version 1. <http://www.pymol.org>.
33. Bhat, S.Y., Dey, A. and Qureshi, I.A. (2018) Structural and functional highlights of methionine aminopeptidase 2 from *Leishmania donovani*. *Int J Biol Macromol*. **115**, 940-954.
34. Trott, O. and Olson, A.J. (2010) AutoDock Vina: improving the speed and accuracy of docking with a new scoring function, efficient optimization, and multithreading. *J Comput Chem*. **31**, 455-61.
35. Yen, C., Green, L. and Miller, C.G. (1980) Degradation of intracellular protein in *Salmonella typhimurium* peptidase mutants. *J Mol Biol*. **143**, 21-33.
36. Chen, X., Chong, C.R., Shi, L., Yoshimoto, T., Sullivan, D.J. Jr. and Liu, J.O. (2006) Inhibitors of *Plasmodium falciparum* methionine aminopeptidase 1b possess antimalarial

- activity. Proc Natl Acad Sci U S A. **103**, 14548-53.
37. Morty, R.E. and Morehead, J. (2002) Cloning and characterization of a leucyl aminopeptidase from three pathogenic *Leishmania* species. J Biol Chem. **277**, 26057-65.
 38. Timm, J., Valente, M., García-Caballero, D., Wilson, K.S. and González-Pacanowska, D. (2017) Structural characterization of acidic M17 leucine aminopeptidases from the TriTryps and evaluation of their role in nutrient starvation in *Trypanosoma brucei*. mSphere. **2**, e00226-17.
 39. Modak, J.K., Rut, W., Wijeyewickrema, L.C., Pike, R.N., Drag, M. and Roujeinikova, A. (2016) Structural basis for substrate specificity of *Helicobacter pylori* M17 aminopeptidase. Biochimie. **121**, 60-71.
 40. Lowther, W.T. and Matthews, B.W. (2000) Structure and function of the methionine aminopeptidases. Biochim Biophys Acta. **1477**, 157-67.
 41. Harbut, M.B., Velmourougane, G., Dalal, S., Reiss, G., Whisstock, J.C., Onderk, O., et al. (2011) Bestatin-based chemical biology strategy reveals distinct roles for malaria M1- and M17-family aminopeptidases. Proc Natl Acad Sci U S A. **108**, E526-34.
 42. Lee, J.Y., Song, S.M., Seok, J.W., Jha, B.K., Han, E.T., Song, H.O., et al. (2010) M17 leucine aminopeptidase of the human malaria parasite *Plasmodium vivax*. Mol Biochem Parasitol. **170**, 45-8.
 43. Dong, L., Cheng, N., Wang, M.W., Zhang, J., Shu, C. and Zhu, D.X. (2005) The leucyl aminopeptidase from *Helicobacter pylori* is an allosteric enzyme. Microbiology. **151**, 2017-23.
 44. Luckett, J.C., Darch, O., Watters, C., Abuoun, M., Wright, V., Paredes-Osses, E., et al. (2012) A novel virulence strategy for *Pseudomonas aeruginosa* mediated by an autotransporter with arginine-specific aminopeptidase activity. PLoS Pathog. **8**, e1002854.
 45. Marschner, A. and Klein, C.D. (2015) Metal promiscuity and metal-dependent substrate preferences of *Trypanosoma brucei* methionine aminopeptidase 1. Biochimie. **115**, 35-43.
 46. Kleifeld, O., Rulísek, L., Bogin, O., Frenkel, A., Havlas, Z., Burstein, Y., et al. (2004) Higher metal-ligand coordination in the catalytic site of cobalt-substituted *Thermoanaerobacter brockii* alcohol dehydrogenase lowers the barrier for enzyme catalysis. Biochemistry. **43**, 7151-61.

47. Kim, H. and Lipscomb, W.N. (1993) X-ray crystallographic determination of the structure of bovine lens leucine aminopeptidase complexed with amastatin: formulation of a catalytic mechanism featuring a gem-diolate transition state. *Biochemistry*. **32**, 8465-78.
48. Chevrier, B., D'Orchymont, H., Schalk, C., Tarnus, C. and Moras, D. (1996) The structure of the *Aeromonas proteolytica* aminopeptidase complexed with a hydroxamate inhibitor. Involvement in catalysis of Glu151 and two zinc ions of the co-catalytic unit. *Eur J Biochem*. **237**, 393-8.
49. Kumar, V.; Sharma, N.; Bhalla, T. C. (2014) In silico analysis of β -galactosidases primary and secondary structure in relation to temperature adaptation. *J Amino Acids*. **2014**, 475839.
50. Cha, M.H., Yong, W.M., Lee, S.M., Lee, Y.S. and Chung, I.Y. (2000) The biochemical and molecular characterization of recombinant *Bacillus subtilis* tripeptidase (PepT) as a zinc-dependent metalloenzyme. *Mol Cells*. **10**, 423-31.
51. Miller, C.G., Miller, J.L. and Bagga, D.A. (1991) Cloning and nucleotide sequence of the anaerobically regulated pepT gene of *Salmonella typhimurium*. *J Bacteriol*. **173**, 3554-8.
52. Tan, P.S., Pos, K.M. and Konings, W.N. (1991) Purification and characterization of an endopeptidase from *Lactococcus lactis* subsp. *cremoris* Wg2. *Appl Environ Microbiol*. **57**, 3593-9.
53. Savijoki, K. and Palva, A. (2000) Purification and molecular characterization of a tripeptidase (PepT) from *Lactobacillus helveticus*. *Appl Environ Microbiol*. **66**, 794-800.

Table 1. Secondary structure and thermostability parameters of PepT and mutazymes based on Far-UV CD spectral data

Enzyme	α -helices	β -sheets	others	T _m (K)
PepT	29	21	50	325.6
T364A	27	23	50	320.5
N378A	25	24	51	318
T364A/N378A	26	23	51	321

Table 2. Effect of divalent metal chlorides on the aminopeptidase activity of PepT

Metal	Concentration (mM)	K _m (μM)	k _{cat} (min ⁻¹)	k _{cat} /K _m × 10 ³ (M ⁻¹ min ⁻¹)
CoCl ₂	0.05	906.1 ± 76.7	9.8 ± 0.73	10.81 ± 1.21
MnCl ₂	0.10	319.9 ± 31.9	4.53 ± 0.36	14.16 ± 1.80
NiCl ₂	0.05	190.8 ± 23.6	1.36 ± 0.07	7.12 ± 0.95
MgCl ₂	10.0	120.4 ± 21.3	2.52 ± 0.14	20.93 ± 3.88
CaCl ₂	10.0	190.3 ± 16.5	3.25 ± 0.13	17.07 ± 1.63
CuCl ₂	0.01	215.4 ± 19.7	1.96 ± 0.14	9.09 ± 1.05
FeCl ₂	0.05	301.4 ± 40.5	2.48 ± 0.27	8.22 ± 1.42
ZnCl ₂	0.0001	394.0 ± 33.2	3.13 ± 0.50	7.94 ± 1.43

Table 3. Steady-state kinetic parameters of PepT and mutazymes for the hydrolysis of peptide substrates

Enzyme	Substrate	K_m (μM)	k_{cat} (min^{-1})	$k_{cat}/K_m \times 10^3$ ($\text{M}^{-1}\text{min}^{-1}$)
PepT	Ala-AMC	906.1 ± 76.7	9.8 ± 0.73	10.81 ± 1.21
PepT	Leu-AMC	49.4 ± 6.2	0.357 ± 0.01	7.22 ± 0.92
PepT	Met-AMC	24.9 ± 3.0	0.146 ± 0.00	5.86 ± 0.70
PepT	Arg-AMC	240.1 ± 23.2	1.802 ± 0.08	7.50 ± 0.79
PepT	Lys-ala-AMC	41.0 ± 5.0	1.56 ± 0.08	38.04 ± 5.03
PepT	Ala-ala-phe-AMC	578.8 ± 51.8	0.521 ± 0.06	0.90 ± 0.13
PepT	Ala-leu-lys-AMC	282.2 ± 21.3	0.089 ± 0.01	0.31 ± 0.04
T364A	Ala-AMC	666.5 ± 50.1	1.68 ± 0.13	2.52 ± 0.27
T364A	Leu-AMC	14.9 ± 1.3	0.081 ± 0.00	5.43 ± 0.47
T364A	Met-AMC	16.2 ± 2.1	0.046 ± 0.01	2.83 ± 0.71
T364A	Arg-AMC	175.0 ± 12.9	0.266 ± 0.02	1.52 ± 0.16
T364A	Lys-ala-AMC	62.8 ± 5.1	1.00 ± 0.04	15.92 ± 1.44
T364A	Ala-ala-phe-AMC	248.5 ± 20.2	0.16 ± 0.01	0.64 ± 0.04
T364A	Ala-leu-lys-AMC	300.6 ± 24.1	0.053 ± 0.00	0.17 ± 0.01
N378A	Ala-AMC	320.7 ± 19.7	0.266 ± 0.02	0.82 ± 0.08
N378A	Leu-AMC	62.5 ± 10.7	0.058 ± 0.01	0.92 ± 0.22
N378A	Met-AMC	13.6 ± 2.2	0.02 ± 0.00	1.47 ± 0.23
N378A	Arg-AMC	98.6 ± 7.1	0.113 ± 0.00	1.14 ± 0.08
N378A	Lys-ala-AMC	63.0 ± 7.8	0.723 ± 0.05	11.47 ± 1.62
N378A	Ala-ala-phe-AMC	622.8 ± 46.6	0.27 ± 0.03	0.43 ± 0.05
N378A	Ala-leu-lys-AMC	235.3 ± 14.6	0.056 ± 0.00	0.23 ± 0.01
T364A/N378A	Ala-AMC	754.6 ± 58.3	6.183 ± 0.14	8.19 ± 0.62
T364A/N378A	Leu-AMC	42.7 ± 4.8	0.266 ± 0.01	6.22 ± 0.73
T364A/N378A	Met-AMC	47.5 ± 4.4	0.136 ± 0.00	2.86 ± 0.26
T364A/N378A	Arg-AMC	324.1 ± 31.5	1.497 ± 0.13	4.61 ± 0.60
T364A/N378A	Lys-ala-AMC	35.5 ± 4.0	1.532 ± 0.07	43.15 ± 5.24
T364A/N378A	Ala-ala-phe-AMC	294.8 ± 26.7	0.416 ± 0.02	1.41 ± 0.14
T364A/N378A	Ala-leu-lys-AMC	151.2 ± 15.6	0.116 ± 0.00	0.76 ± 0.08

Table 4. IC-50 values of PepT and its mutants with different aminopeptidase inhibitors.

Enzyme	Arphamenine A (μM)	Bestatin (μM)	Actinonin (nM)	Amastatin (nM)
PepT	98.66 ± 6.51	4.47 ± 0.65	24.78 ± 2.86	6.46 ± 0.70
T364A	74.72 ± 4.70	2.29 ± 0.27	14.36 ± 1.87	5.61 ± 0.63
N378A	120.40 ± 9.31	7.59 ± 1.13	24.03 ± 3.10	10.58 ± 1.16
T364A/ N378A	152.90 ± 12.33	11.45 ± 1.24	24.35 ± 2.68	10.47 ± 1.28

Table 5. Dissociation rate constant (K_D) of bimolecular interactions between various peptide substrates and enzymes PepT and N378A.

Ligand	Analyte	K_D (M)
PepT	Lys-ala-AMC	2.95×10^{-8}
N378A	Lys-ala-AMC	4.43×10^{-7}
PepT	Ala-leu-lys-AMC	5.08×10^{-5}
N378A	Ala-leu-lys-AMC	2.37×10^{-4}
PepT	Met-AMC	3.59×10^{-7}
N378A	Met-AMC	1.02×10^{-5}

Figure legends:**Figure 1: Domain organisation, multiple sequence alignment and homology modelling.**

(A) Domain architecture of PepT highlighting its two domains and a sub-domain. NTCD (grey, residues 1-218) and LD (blue, residues 219-330) stand for N-terminal catalytic domain and lid domain, respectively. The NTCD (residues 330-416) towards the C-terminal end represents a sub-domain which in 3D structure of PepT recoils onto the C-terminal NTCD. (B) Alignment of leishmanial PepT sequence with ortholog sequences from bacteria. The secondary structure highlighted in the alignment corresponds to the secondary structure seen in the modelled structure of PepT. The helices and sheets are shown by black coils and arrows, respectively. The conserved residues between sequences are shown in red and semi-conserved residues in yellow. The metal interacting residues are highlighted by blue stars. These residues make up the co-catalytic core with two divalent cations (Zinc) along with the H85 and H387. Conserved substrate binding residues (T364 and N378) of PepT family are highlighted by black upright triangles. (C) Homo-dimer of PepT with each monomer labelled as A and B. The two metal ions can be seen in grey colour as spheres in both monomers. (D) Residues D147, E181 and D205 shown in sticks can be seen interacting with two divalent metal ions (shown as grey spheres) in the catalytic centre. (E) Alignment of PepT (red), T364A (blue), N378A (black) and T364A/N378A (green) structures demonstrating rotameric changes in metal interacting residues which are shown as sticks. Two metal ions are displayed as grey spheres.

Figure 2: Purification and biophysical characterization. (A) Pre-stained marker is denoted by letter M. Purification of PepT (lane 1) and its mutazymes T364A (lane 2), N378A (lane 3) and T364A/N378A (lane 4) on a 10% (w/v) SDS-PAGE gel. (B) Gel filtration chromatographic elution profile of PepT. (C) Far-UV CD spectra of PepT and mutazymes. (D) Heat-denaturation plots of PepT and mutazymes depicting a shift in melting temperatures after mutations. (E) Fluorescence spectra of PepT and mutazymes.

Figure 3: Metal dependence and biochemical highlights of PepT. (A) Metal promiscuity and metal dependence of PepT highlighting that the different metal chlorides activate this enzyme optimally at different concentrations. (B) Analysis of pH dependence of PepT in the pH range of 3.5 to 9.5. (C) Assessment of the optimal temperature for the aminopeptidase activity of PepT. (D-K) Michaelis-Menten fit for the aminopeptidase assay of PepT and

mutazymes against peptides linked to fluorophore AMC. Data indicates the mean activity \pm SD (n=3).

Figure 4: Inhibition of PepT. (A, E, I and M) Lineweaver-Burk plots showing the competitive mode of inhibition of PepT with arphamenine A, bestatin, actinonin and amastatin. (B, F, J, N) Computation of inhibition constant (K_i). Figures (C, G, K and O) depict the relative inhibition of PepT and mutazymes by aminopeptidase inhibitors. Figures (D, H, L and P) display the atomic interactions of inhibitors with PepT at its catalytic active site. Inhibitors and interacting residues are given in sticks. Black discontinuous lines in the figure display hydrogen bonding and grey spheres represent divalent zinc. Other residues represented as sticks in the figures have hydrophobic interactions with inhibitors. The biochemical data is presented as mean \pm SD of three independent experiments.

Figure 5: Surface plasmon resonance. (A-F) SPR sensorgrams depicting bimolecular interactions between peptide substrates and enzymes PepT and N378A. The data is presented as mean of two independent experiments performed at room temperature.

Figure 6: Structural basis of substrate specificity of PepT. Cartoon representation of the homo-dimeric structure of PepT with binding poses of substrates Ala-AMC (red coloured sticks), Lys-ala-AMC (cyan coloured sticks) and Ala-ala-phe-AMC (magenta coloured sticks). Active site and substrate binding sites are shown by arrows. Atomic interactions involved in the binding of Ala-AMC (A), Lys-ala-AMC (B) and Ala-ala-phe-AMC (C). Structural coordinates of peptide substrates and interacting residues of PepT are displayed as sticks. Black dashed lines display hydrogen bonding. Grey spheres represent two metal ions.

Figure 7: Molecular dynamic simulations and MM/PBSA. Figures (A), (B) and (C) show the RMSD, RMSF and Rg of native PepT and PepT-Ala-AMC complex during 20ns MDS run. (D) Interactions of Ala-AMC with PepT at the catalytic centre at t=20ns. (E), (F) and (G) RMSD, RMSF and Rg plot of T364A and its complex with Ala-AMC. (H) Network of interactions between mutazyme T364A and Ala-AMC. (I), (J) and (K) display the RMSD, RMSF and Rg plot of N378A and its complex with Ala-AMC. (L) Interactions of Ala-AMC with residues D205, E181 and C207 at the catalytic centre of N378A. Substrate and interacting residue side-chains are shown in sticks. (M), (N) and (O) RMSD, RMSF and Rg plot of mutazyme T364A/N378A and its complex with Ala-AMC. (P) Interactions of Ala-

AMC with T364A/N378A. (Q) MM/PBSA binding energy profile of PepT and its mutazymes highlighting the highest binding energy of peptide substrate Ala-AMC with PepT.

- Metal-dependent peptidase T (PepT) exists as homo-dimer in solution and shows high catalytic efficiency for the hydrolysis of peptides carrying alanine at the P¹ position.
- Actinonin and amastatin inhibit PepT potently in low nanomolar range, while arphamenine A and bestatin are effective only in micromolar concentrations.
- A double mutant (T364A/N378A) of PepT cleaves peptides carrying a bigger P¹ residue emerging as a catalytically efficient broad-spectrum aminopeptidase.
- Surface plasmon resonance and MM/PBSA free energy calculations demonstrate lesser substrate binding of PepT mutants to be a key reason for amidolytic digressions.